International Geology Review

ISSN: 0020-6814 (Print) 1938-2839 (Online) Journal homepage: https://www.tandfonline.com/loi/tigr20

Grenville-age metamorphism in the Larsemann Hills: P-T evolution of the felsic orthogneiss in the Broknes Peninsula, East Antarctica

Shi Zong, Liudong Ren & Meiqian Wu

To cite this article: Shi Zong, Liudong Ren & Meiqian Wu (2020): Grenville-age metamorphism in the Larsemann Hills: P-T evolution of the felsic orthogneiss in the Broknes Peninsula, East Antarctica, International Geology Review, DOI: 10.1080/00206814.2020.1734973

To link to this article: https://doi.org/10.1080/00206814.2020.1734973

Published online: 10 Mar 2020.

INTERNATIONAL GEOLOGY REVIEW
https://doi.org/10.1080/00206814.2020.1734973

Taylor & Francis
Taylor & Francis Group

ARTICLE

Grenville-age metamorphism in the Larsemann Hills: P-T evolution of the felsic orthogneiss in the Broknes Peninsula, East Antarctica

Shi Zong[a,b], Liudong Ren[a] and Meiqian Wu[c]

[a]Institute of Geology, Chinese Academy of Geological Sciences, Beijing, China; [b]Chinese Academy of Geological Sciences, China University of Geosciences, Beijing, China; [c]School of Earth Sciences and Engineering, Nanjing University, Nanjing, China

ABSTRACT

The gneisses outcropping in the Larsemann Hills of East Antarctica are ideal for studying the composition and evolution of the Prydz tectonic belt. In this study, detailed petrological analyses, phase equilibrium modelling, and zircon analyses were performed on a felsic orthogneiss from the Broknes Peninsula in the Larsemann Hills. The study results show that the protolith of the felsic gneiss is granite, which is further identified to have been an S-type granitoid. The felsic orthogneiss intruded into the basement complex at ~976 Ma. The magmatic zircons in the felsic orthogneiss have lower LREE and higher HREE contents than those of the metamorphic zircons in the same rock. The felsic gneiss consists of the mineral assemblage garnet +ilmenite+ plagioclase +K-feldspar + sillimanite + quartz and underwent granulite facies metamorphism in the Grenvillian period (~899 Ma), with peak conditions of ~870°C and ~9.5 kbar. The Larsemann Hills should be categorized as the orogenic process from arc-continent collision to continent-continent collision during the Grenvillian period, crust thickening(~899 Ma) and subsequent collapse(550–500 Ma).

ARTICLE HISTORY
Received 28 August 2019
Accepted 23 February 2020

KEYWORDS
East Antarctica; felsic gneisses; pseudosection modelling; zircon U-Pb geochronology; zircon REE and Lu-Hf characteristics; Grenvillian event

1. Introduction

There are different perspectives on the tectonic evolution of Prydz Bay of East Antarctica: P-T paths with clockwise near isothermal decompression (ITD) indicate that it is a Pan-African collision orogeny related to crustal thickening (Ren *et al*. 1992, 2018; Fitzsimons 1996; Carson *et al*. 1997; Yu *et al*. 2002; Liu *et al*. 2006, 2007a, 2007b, 2007c; Hu *et al*. 2008). The creation of Prydz Bay is related to the final convergence of the East Gondwana continent (Zhao *et al*. 1993, 2003; Hensen and Zhou 1997; Fitzsimons 2000; Liu *et al*. 2002a, 2002b, 2007a, 2007b, 2007c, 2018; Harley 2003; Hu *et al*. 2008). Prydz Bay has experienced not only a Grenvillian (~1000 Ma) metamorphic event, but also a Pan-African (~530 Ma) tectonic thermal event (Dirks and Hand 1995; Liu *et al*. 1995, 2007b, 2009a; Zhang *et al*. 1996; Tong *et al*. 1998, 2002, 2017; Tong and Wilson 2006; Wang *et al*. 2008; Grew *et al*. 2012; Zhou *et al*. 2014). However, there is still much controversy regarding the distribution of these two tectonic events in this area and their geological significance. Some scholars hold that the P-T paths of these two metamorphic events are not related (Dirks and Hand 1995; Tong *et al*. 1998, 2002; Kelsey *et al*. 2007; Wang *et al*. 2007, 2008). Therefore, the Prydz belt is also considered to represent an intracontinental activity belt active in the Early Palaeozoic in Eastern Gondwana. It may be the result of the tectonic adjustment effect of the collision between two parts of the Gondwana continent (Tong *et al*. 2002; Phillips *et al*. 2007; Wang *et al*. 2007, 2008; Wilson *et al*. 2007; Grew *et al*. 2012; Ren *et al*. 2018). However, others believe that the two tectonic metamorphic events represent the aggregation of the continents of Rodinia and Gondwana, respectively, and that the Prydz tectonic belt is a collisional orogenic belt (Hensen and Zhou 1997; Fitzsimons 2000; Boger *et al*. 2001; Liu *et al*. 2002b, 2006; Zhao *et al*. 2003; Li and Liu 2006). Resolving these differences in perspectives is important for understanding how the East Antarctic continent formed. The Larsemann Hills are located in the heart of Prydz Bay, and the Broknes Peninsula is a major part of the Larsemann Hills. Therefore, an in-depth study of the rocks at these locations is important for establishing a complete metamorphic P-T path in this area, and is of great significance to clarify the metamorphic thermal evolution and tectonic nature of Prydz Bay.

2. Geological background

The Larsemann Hills is located in Prydz Bay in East Antarctica and is underlain by composite orthogneiss (mafic and felsic orthogneiss) and metasedimentary

CONTACT Liudong Ren ldren@cags.ac.cn Institute of Geology, Chinese Academy of Geological Sciences, Beijing, 103007, China

rocks, known as the Søstrene Orthogneiss and Brattstrand Paragneiss, respectively (Fitzsimons *et al*. 1997). After peak metamorphism, the anatexis was strongly developed in this region, and a considerable number of pegmatite veins, migmatites and garnet-bearing granites were formed along with the local syenite porphyry and monzonitic granite and ultramafic granulite (Carson *et al*. 1995, 2010; Grew *et al*. 2012; Tong *et al*. 2017). The Søstrene Orthogneiss and the Brattstrand Paragneiss are considered to be basement series and sedimentary cover rocks, respectively (Sheraton *et al*. 1984; Stüwe and Powell 1989; Fitzsimons and Harley 1991; Dirks *et al*. 1993; Carson *et al*. 1995; Dirks and Hand 1995) (Figure 1).

The Larsemann Hills experienced D_1 deformation and granulite facies metamorphism in the Grenvillian period and D_2-D_6 phases of deformation and amphibolite to granulite facies metamorphism in the Pan-African stage (Dirks *et al*. 1993). Wang *et al*. (2008) summarized the major geological events in the Larsemann Hills (Table 1). They believed that the D_1 deformation was accompanied by early (~1000 Ma) granulite facies metamorphism and intrusion of syn-orogenic granite. There is also a granulite facies metamorphism event in the Pan-African period (~500 Ma) with strong anatexis, simultaneous D_2 northwestward thrust and D_3 north-south extension deformation, and intrusion of syn-orogenic granite. Ren *et al*. (1992) obtained the peak metamorphic conditions of the early M_1 (The M_1 corresponds to the D_1) corresponding to 9 kbar and 850°C using the Grt-Pl-Sil-Qz geothermobarometer and Opx-Cpx thermometer. Tong *et al*. (1995) stated that the early M_1 reached higher peak metamorphic conditions of 9.5 kbar and 870°C (Grt-Opx geothermobarometer). The Pan-African tectonic activity exhibited amphibolite to granulite facies metamorphism and the peak metamorphism conditions were 7 kbar and 800–850°C (Carson *et al*. 1995, 1997; Fitzsimons 1996; Grew *et al*. 2006). Recently, the early M1 conditions of 9.3 kbar and 900–950°C are also reported from the garnet-bearing mafic granulite in the study region (Tong *et al*. 2019)

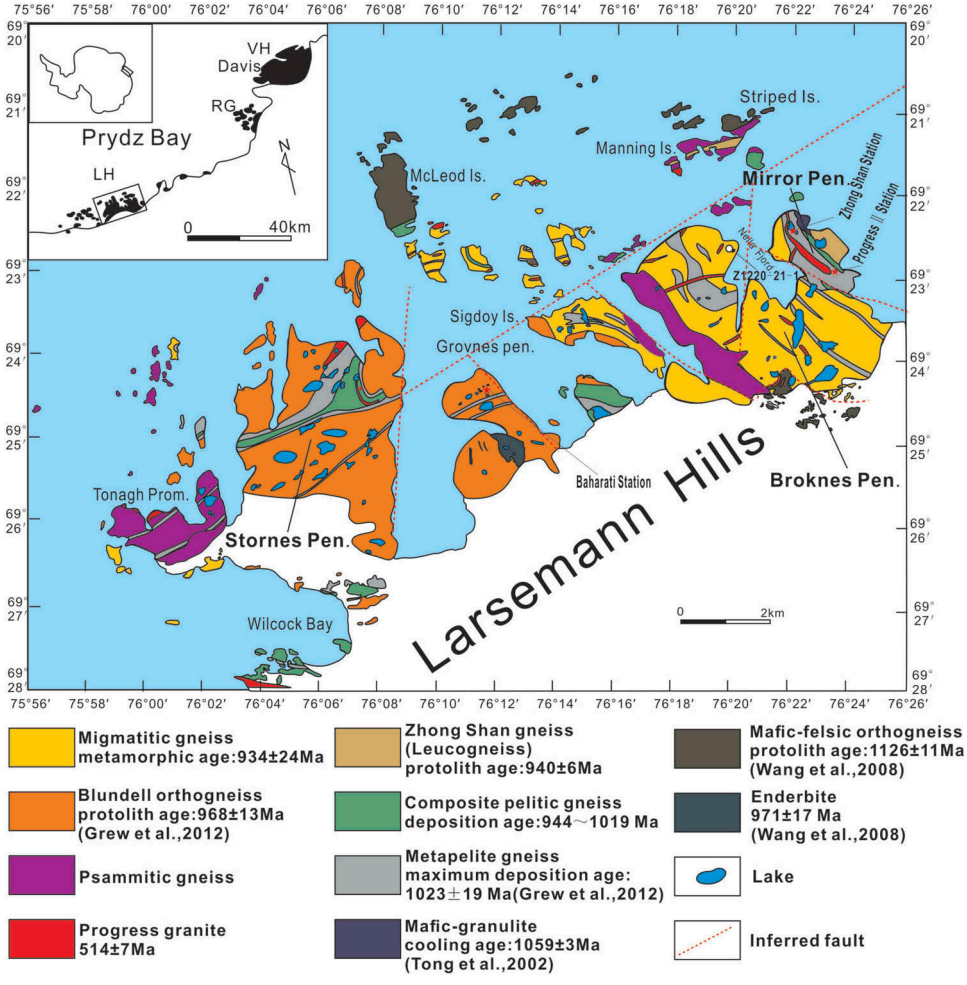

Figure 1. Geological map of the Larsemann Hills, Prydz Bay, East Antarctica and the sample locations, showing major lithological units (after Tong *et al*. (2017)). Insert shows the position of the Larsemann Hills in Prydz Bay. Abbreviations: LH, Larsemann Hills, RG, Rauer group, VH, Vestfold Hills.

Table 1. The main geological events in the Larsemann Hills and its adjacent regions, East Antarctica (after Wang *et al*. (2008).

Pan-African	Dalkoy granite	501 ± 11 Ma
	Pegmatite	504 ± 17 Ma
	Progress granite	516 ± 7 Ma
	Leucogranite	524 ± 20 Ma
	D3: N-S extension event	
	D2: WNW-directed thrusting event, M2: granulite	529 ± 8 Ma
Grenvillian	Enderbite intrusion	971 ± 17 Ma
	Granitic gneiss intrusion	ca.1000 Ma (~975 Ma our data)
	D1: interleaving of mafic-felsic gneiss and	ca.1000 Ma
	Sedimentary rocks, M1: Granulite-facies	(~910 Ma our data)
	Metasedimentary rocks (pelite, psammite, quartzite, etc.)	
	Felsic intrusives	ca.1100 Ma

However, the relationship between the early Grenvillian and late Pan-African tectonic activity is complicated.

3. Analytical methods

Analysis of the major elements and trace elements were performed at the Special Laboratory of the Geological Team of Hebei Province, Langfang, China. The major oxides were determined by X-ray fluorescence (XRF) on fused glass beads and the trace elements were analysed using a Perkin-Elmer Sciex Elan 6000 ICP-MS. Samples were dissolved using a mixture of HNO_3 and HF. Specific test conditions and steps can be found in Jin and Zhu (2000).

The zircons were extracted from the samples by a manual extraction method under a binocular microscope. They were then mounted in epoxy resin discs, and sectioned and polished to reveal their cross section. Cathodoluminescence (CL) imaging of zircon particles was performed using a JSM6510 scanning electron microscope (SEM; JEOL, Tokyo Japan) attached to a Gatan CL detector (Oxford, UK) at Nanjing Hongchuang Geological Exploration Technology Service Co., Ltd, China. U-Pb dating analyses were conducted using laser-ablation–inductively coupled plasma–mass spectrometry (LA–ICP–MS) at the Beijing Createch Test Technology Co. Ltd., China. Laser sampling was performed using an ESI NWR 193 nm laser ablation system and an Anlyitik Jena PQMS Elite ICP-MS instrument was used to acquire ion-signal intensities. Detailed operating conditions are the same as described by Hou *et al*. (2009). Off-line raw data selection and integration of background and analyte signals, and time-drift correction and quantitative calibration for U-Pb dating was performed using ICPMS DataCal (Liu *et al*. 2010). The age calculations and Concordia diagrams were made using Isoplot (Ludwig 2003). Lu-Hf isotopes were analysed in situ in the same age zones in zircon that were analysed for U-Pb isotopes. The analyses were performed using a Neptune MC–ICP–MS equipped with a GeoLas 200 M ArF excimer 193 nm laser ablation system (MicroLas, Germany).

Electron probe micro-analysis (EPMA) of minerals was carried out on polished thin sections at the State Key Laboratory for Mineral Deposits Research of Nanjing University. A JEOL JXA-8100 electron probe micro-analyser was used with an accelerating voltage of 15 kV, and cup current of 20 nA and 1 μm for the minerals. The test results are shown in Table 2–4.

4. Petrography and mineral chemistry

The felsic gneiss (sample Z1220-21-1) studied in this paper was collected near the Nella Fjord in the Broknes Peninsula (Figure 1). Through outcrops we can see that it intrudes into the basement complex, and has a porphyroblastic texture, contains locally-developed feldspar quartz veins (Figure 2(a)). The main minerals of the felsic gneiss are coarse-grained K-feldspar (20%), plagioclase (25%), biotite (5%), garnet (15%), and quartz (45%); a small amount of sillimanite, muscovite, magnetite and ilmenite are also present(Figure 2(b)). Garnet forms euhedral porphyroblasts with diameters of more than 1 mm in the felsic orthogneiss.Most of the sillimanite and biotite are found along the grain boundaries of the other minerals (Figure 2(c)). The Sil and Bi may be late stage minerals. Based on the minerals in the garnets and in the matrix, two-stage mineral assemblages can be ascertained: 1) The prograde stage is characterized by the mineral assemblage of muscovite (Ms)+ biotite (Bi) + plagioclase (Pl) + microcline (Mic) + quartz (Qz) + magnetite (Mgt) occurring as inclusions in garnet. 2) The peak metamorphism stage (M_1) is defined by the mineral assemblage of garnet (Grt) + ilmenite (Ilm) + plagioclase (Pl) + K-feldspar (Kfs) + sillimanite (Sil) + quartz (Qz)

The results of the electron microprobe analysis show that the garnet in the felsic gneiss has high FeO and MgO, low CaO, and almost no MnO (Table 2). The garnet has a composition of $Alm_{69\text{-}73}Py_{25\text{-}27}Gr_{2\text{-}3}$, without substantial compositional zoning from core to rim (Figure 3(a,b)).

The amount of biotite in the samples is low, and only a small amount of residual crystals are present. The outlines of the biotite grains are certainly irregular – the grains look embayed. (Figure 2(b)). Electron probe data show that the biotite has high MgO and TiO_2, but lacks MnO. The feldspar in the sample is mainly microcline and plagioclase. There are two types of microcline: one type is distributed at the edges of the garnet, while the other exists in the matrix together with biotite, quartz, plagioclase. The plagioclase is mainly encircled in the interior of the perthite, either in the matrix or between them. Some are irregularly surrounded by garnet and a small

Table 2. Reprersentative microprobe analyses of garnet of the sample(wt%).

sample	Z1220-21-1																
Spot	1	2	3	4	5	6	7	8	10	11	12	13	14	15	16	17	9
Location	Rim							Core									Rim
SiO_2	39.18	39.19	39.29	38.58	38.87	40.30	38.33	38.76	39.07	39.99	39.08	39.01	38.28	38.79	39.16	39.22	38.32
TiO_2	0.01	0.00	0.07	0.05	0.02	0.03	0.00	0.00	0.03	0.02	0.06	0.05	0.07	0.06	0.06	0.05	0.01
Al_2O_3	21.55	21.19	21.57	21.14	21.39	22.16	21.40	21.14	21.41	21.72	21.75	21.51	21.09	21.11	21.63	21.73	21.24
FeO	31.08	31.35	30.72	32.14	31.84	31.17	31.42	30.48	31.77	31.14	31.07	31.18	31.82	31.04	31.45	31.45	31.95
MnO	0.08	0.04	0.11	0.06	0.06	0.05	0.07	0.10	0.07	0.08	0.09	0.08	0.09	0.07	0.06	0.06	0.08
MgO	6.70	6.73	6.68	6.35	6.04	6.80	6.57	6.75	6.56	6.66	6.50	6.69	6.47	6.60	6.28	6.61	6.42
CaO	0.84	0.87	0.91	0.92	0.96	1.00	1.02	1.00	1.02	0.99	1.01	0.98	0.97	0.92	0.88	0.86	1.01
Na_2O	0.00	0.00	0.01	0.06	0.00	0.01	0.07	0.00	0.01	0.00	0.05	0.01	0.02	0.02	0.00	0.03	0.02
Total	99.42	99.36	99.35	99.30	99.18	101.51	98.87	98.23	99.93	100.60	99.60	99.51	98.81	98.61	99.51	100.00	99.05
Listed below is the formula with Fe3+ corrected according to Droop (1987, Mineralogical Magazine, v. 51, pp. 431–435)																	
Si	3.09	3.09	3.10	3.05	3.08	3.11	3.04	3.09	3.07	3.11	3.07	3.07	3.04	3.08	3.09	3.07	3.04
Ti	0.00	0.00	0.00	0.00	0.00	0.00	0.00	0.00	0.00	0.00	0.00	0.00	0.00	0.00	0.00	0.00	0.00
Al	2.00	1.97	2.00	1.97	2.00	2.01	2.00	1.99	1.98	1.99	2.02	2.00	1.98	1.98	2.01	2.01	1.99
Fe^{3+}	0.00	0.00	0.00	0.00	0.00	0.00	0.00	0.00	0.00	0.00	0.00	0.00	0.00	0.00	0.00	0.00	0.00
Fe^{2+}	2.03	2.06	2.01	2.12	2.10	1.99	2.08	2.02	2.08	2.01	2.03	2.04	2.11	2.05	2.06	2.05	2.11
Mn	0.01	0.00	0.01	0.00	0.00	0.00	0.00	0.01	0.00	0.01	0.01	0.01	0.01	0.00	0.00	0.00	0.01
Mg	0.79	0.79	0.79	0.75	0.71	0.78	0.78	0.80	0.77	0.77	0.76	0.79	0.77	0.78	0.74	0.77	0.76
Ca	0.07	0.07	0.08	0.08	0.08	0.08	0.09	0.09	0.09	0.08	0.08	0.08	0.08	0.08	0.07	0.07	0.09
Na	0.00	0.00	0.00	0.01	0.00	0.00	0.01	0.00	0.00	0.00	0.01	0.00	0.00	0.00	0.00	0.00	0.00
Total	7.99	7.99	7.98	7.99	7.98	7.98	7.99	7.99	7.99	7.98	7.99	7.99	7.99	7.99	7.98	7.99	7.99
alm	0.70	0.70	0.70	0.72	0.73	0.70	0.71	0.69	0.71	0.70	0.71	0.70	0.71	0.70	0.72	0.71	0.71
sps	0.00	0.00	0.00	0.00	0.00	0.00	0.00	0.00	0.00	0.00	0.00	0.00	0.00	0.00	0.00	0.00	0.00
py (Mg#)	0.27	0.27	0.27	0.25	0.25	0.27	0.26	0.27	0.26	0.27	0.26	0.27	0.26	0.27	0.26	0.27	0.26
gr	0.02	0.03	0.03	0.03	0.03	0.03	0.03	0.03	0.03	0.03	0.03	0.03	0.03	0.03	0.03	0.02	0.03

Table 3. Reprersentative microprobe analyses of biotite of the sample(wt%).

sample	Z1220-21-1												
SiO_2	38.13	38.45	37.56	37.96	37.47	38.90	37.21	37.59	36.92	36.44	37.51	36.77	38.18
TiO_2	5.54	5.24	5.47	5.23	5.59	3.79	5.19	6.16	4.72	5.00	5.45	5.23	4.48
Al_2O_3	14.78	15.36	14.79	15.02	15.28	15.61	14.96	15.23	15.02	14.74	15.30	14.60	14.43
FeO	14.47	12.98	14.27	14.37	14.93	10.94	14.79	15.91	16.53	17.79	14.76	18.59	16.57
MnO	0.00	0.02	0.01	0.01	0.00	0.01	0.00	0.02	0.00	0.00	0.03	0.01	0.01
MgO	13.95	15.43	13.87	14.11	13.26	17.06	14.32	12.94	12.29	11.21	12.96	10.52	13.40
CaO	0.00	0.00	0.00	0.00	0.00	0.00	0.03	0.00	0.00	0.01	0.00	0.00	0.00
Na_2O	0.06	0.04	0.05	0.03	0.20	0.25	0.24	0.20	0.05	0.09	0.26	0.21	0.16
K_2O	9.49	10.00	9.62	9.57	9.42	9.81	9.16	9.30	9.53	9.46	8.97	9.34	9.46
Total	96.42	97.51	95.64	96.30	96.15	96.37	95.90	97.34	95.06	94.73	95.23	95.27	96.69
Si	2.80	2.78	2.79	2.79	2.77	2.81	2.76	2.75	2.79	2.78	2.79	2.80	2.83
Ti	0.31	0.28	0.30	0.29	0.31	0.21	0.29	0.34	0.27	0.29	0.30	0.30	0.25
Al	1.28	1.31	1.29	1.30	1.33	1.33	1.31	1.32	1.34	1.33	1.34	1.31	1.26
Fe^{2+}	0.89	0.78	0.89	0.88	0.92	0.66	0.92	0.98	1.04	1.13	0.92	1.18	1.03
Mn	0.00	0.00	0.00	0.00	0.00	0.00	0.00	0.00	0.00	0.00	0.00	0.00	0.00
Mg	1.53	1.66	1.53	1.55	1.46	1.84	1.58	1.41	1.38	1.27	1.44	1.19	1.48
Ca	0.00	0.00	0.00	0.00	0.00	0.00	0.00	0.00	0.00	0.00	0.00	0.00	0.00
Na	0.01	0.00	0.01	0.00	0.03	0.03	0.03	0.03	0.01	0.01	0.04	0.03	0.02
K	0.89	0.92	0.91	0.90	0.89	0.90	0.87	0.87	0.92	0.92	0.85	0.91	0.89

number are wrapped in fine granules inside the garnet. The An (~29) of the plagioclase in the matrix is slightly lower than the An (31–35) of the plagioclase in the garnet.

5. P-T estimates and pseudosection calculation

For estimating the metamorphic temperature and pressure conditions, previous studies mostly used the traditional mineral thermobarometers. However, in recent years, increasingly more scholars have begun to use phase equilibrium modelling methods. These methods can not only quantitatively simulate the metamorphic conditions and processes of metamorphism and melting reactions under the actual whole rock chemical composition system, but also quantitatively simulate the content and composition of minerals and melts. In this study, the metamorphic conditions and P-T path of the felsic gneiss were further constrained by phase equilibrium modelling. NCKFMASHTO (Na_2O-CaO—K_2O—FeO—MgO—Al_2O_3—SiO_2—H_2O—TiO_2—O (Fe_2O_3)) P–T pseudosections were computed using GeoPS (Xiang; http://www.geology.ren/), which is a software based on Perple_X (Connolly, version 6.8.4 of

Table 4. Reprersentative microprobe analyses of plagioclase of the sample(wt%).

sample	Z1220-21-1											
Location	in Grt	in Grt	in Grt	in Grt	in Grt	in Grt	in Grt	in Grt	in Grt	in Grt	in matrix	in matrix
K_2O	0.31	0.25	0.24	0.46	0.62	0.40	0.25	0.25	0.56	0.45	0.64	0.66
Na_2O	7.42	7.71	7.16	7.66	7.25	7.52	7.40	7.21	7.70	7.34	7.69	6.63
MnO	0.00	0.00	0.00	0.00	0.00	0.00	0.00	0.02	0.00	0.00	0.00	0.00
TiO_2	0.02	0.00	0.01	0.00	0.02	0.05	0.02	0.01	0.03	0.00	0.03	0.02
MgO	0.01	0.01	0.00	0.01	0.00	0.02	0.00	0.00	0.00	0.02	0.00	1.41
CaO	6.73	6.63	6.90	7.04	6.97	7.09	7.36	7.32	6.59	6.24	6.19	5.29
FeO	0.04	0.06	0.00	0.01	0.02	0.01	0.00	0.01	0.02	0.05	0.01	3.97
Al_2O_3	26.86	27.15	27.19	27.36	27.19	27.21	27.90	27.64	26.88	26.43	26.34	26.20
SiO_2	56.86	57.56	57.55	57.57	57.06	56.84	57.38	56.84	57.81	57.79	58.35	54.26
Total	98.24	99.38	99.03	100.10	99.13	99.14	100.31	99.31	99.58	98.33	99.26	98.43
Si	2.59	2.59	2.59	2.58	2.58	2.57	2.56	2.56	2.60	2.62	2.62	2.51
Ti	0.00	0.00	0.00	0.00	0.00	0.00	0.00	0.00	0.00	0.00	0.00	0.00
Al	1.44	1.44	1.44	1.44	1.45	1.45	1.47	1.47	1.42	1.41	1.40	1.43
Fe^{2+}	0.00	0.00	0.00	0.00	0.00	0.00	0.00	0.00	0.00	0.00	0.00	0.15
Mn	0.00	0.00	0.00	0.00	0.00	0.00	0.00	0.00	0.00	0.00	0.00	0.00
Mg	0.00	0.00	0.00	0.00	0.00	0.00	0.00	0.00	0.00	0.00	0.00	0.10
Ca	0.33	0.32	0.33	0.34	0.34	0.34	0.35	0.35	0.32	0.30	0.30	0.26
Na	0.65	0.67	0.63	0.66	0.64	0.66	0.64	0.63	0.67	0.65	0.67	0.60
K	0.02	0.01	0.01	0.03	0.04	0.02	0.01	0.01	0.03	0.03	0.04	0.04
An	0.33	0.32	0.34	0.33	0.33	0.33	0.35	0.35	0.31	0.31	0.30	0.29
Ab	0.65	0.67	0.64	0.65	0.63	0.64	0.64	0.63	0.66	0.66	0.67	0.66
Or	0.02	0.01	0.01	0.03	0.04	0.02	0.01	0.01	0.03	0.03	0.04	0.04

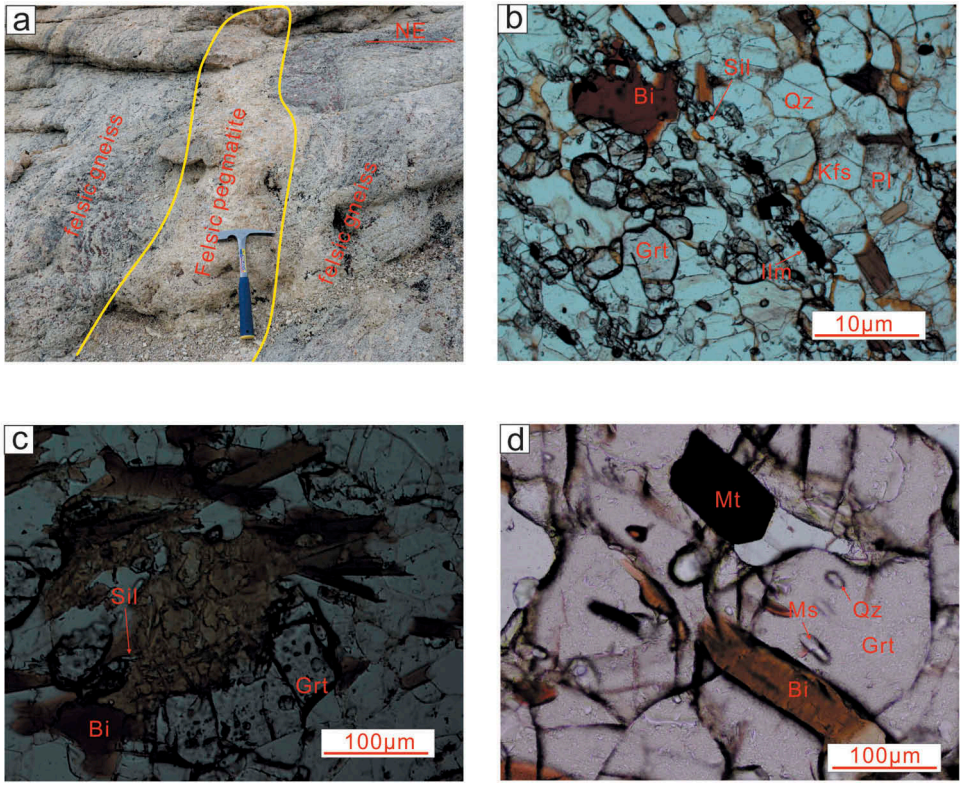

Figure 2. (a) a felsic pegmatite vein in the felsic orthogneiss; (b,c) Photomicrograph of the felsic orthogneiss; (d) Inclusions of biotite (Bi)+quartz (Qz)+muscovite (Ms)+magnetite (Mt) in the garnet.

2015, 2018 upgrade), and the following phases and the corresponding phase components were chosen from Holland and Powell (1998) (Holland and Powell 2011 upgrade). The solution models (details in solution_model.dat; database: hp622ver.dat) adopted are Chl(W), Grt(W), Mica(W), Crd(W), Bi(W), Ctd(W), St(W), melt(W), Fsp(C1), Sp(WPC), Ilm(W), and Melt (HP).The composition used in the phase equilibrium calculation was taken from the full rock composition obtained by XRF analysis. Measured total rock composition is: SiO_2 = 73.72%, TiO_2

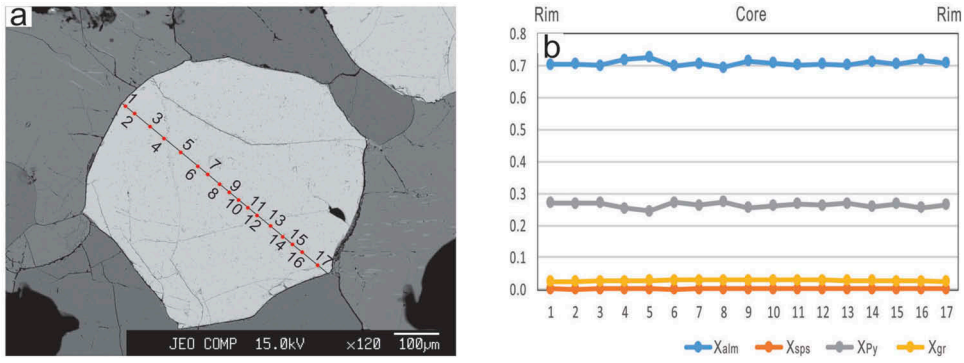

Figure 3. (a) BSE images; (b) compositional profiles of the garnet. Xalm means the composition of the almandine. Xsps means the composition of the spessartine. Xpy means the composition of the pyrope. Xgr means the composition of the grossular.

= 0.2%, Al_2O_3 = 14.01%, K_2O = 6.39%, Na_2O = 2.04%, Fe_2O_3 = 0.05%, FeO = 1.63%, MnO = 0.024%, MgO = 0.31%, CaO = 0.97%, P_2O_5 = 0.095%. The MnO content in the rock is very low (<0.1%), so MnO was not considered in the chemical system chosen for modelling. In addition, CO_2 and P_2O_5 present in the calcium carbonate and apatite were subtracted according to $CaO{\cdot}CO_2$ and $(CaO)5{\cdot}(P_2O_5)1.5(H_2O)0.5$, respectively. We used the T-X(O) pseudosection and the measured mineral assemblage equivalent line to limit the percentage of O (Pownall *et al*. 2015). Calculating the T-X(O) pseudosection of this sample at 6kbar, when the O content was 0.015, ensured that the observed final phase assemblage was stable on the solid phase line (Korhonen *et al*. 2012; Li and Wei 2016). Using a similar method, we obtained a H_2O content of 0.38.

The phase equilibrium modelling temperature and pressure of the sample were limited to the range of 2 ~12 kbar and 500~1100°C. The early metamorphic mineral association (Grt + Ms + Bi + Pl + Ab + Mic + Qz + Mt) is stable in the range of ~ 560°C and 5.2 ~ 8.8 kbar, which represents the prograde metamorphic stage of the rock. The mineral assemblage (Grt + Melt +Ilm+ Pl + Kfs + Sill + Qz) in the peak metamorphic stage is stable at 760 ~ 1050°C and 5 ~ 11.8 kbar. An aqueous fluid is calculated to be present in the system over a pressure-temperature range from about 2.0 to about 5.5 kbar and from about 560 to about 700°C.

According to the pseudosection(Figure 4(a)), rutile is stable at pressures >7.0 ~ 8.8 kbar; cordierite is absent at pressures >5.5 kbar; biotite breaks down at temperatures >700 ~ 760°C; K-feldspar breaks down at temperatures >940 ~ 1000°C. Garnet, quartz and plagioclase are stable over most of the pressure-temperature range covered in the pseudosection except the highest temperatures and lowest pressures where only ilmenite remains. If the isopleths for garnet Mg# are nearly parallel to the pressure axis, then garnet Mg# would change very little with pressure. Figure 4(b) shows garnet Mg# increasing with increasing temperature. If the isopleths for plagioclase An are roughly parallel to the temperature axis, then plagioclase An would not change very much with temperature. Figure 4(b) shows plagioclase An for the most part decreasing with increasing pressure for temperatures above 560–600°C, depending on the pressure. Using the $Mg^{\#}$ of the garnets core to define the P-T condition during the formation of garnets, the $Mg^{\#}$ is 0.261～0.274, and the An of the fine plagioclases inside the garnet is 0.311～0.354. According to the $Mg^{\#}$ of the garnet's core and the An of the plagioclases (0.293 ~ 0.297) in the matrix, the maximum temperature and pressure conditions for the stability of the peak (M_1) mineral combination were T = ~870°C and P = ~9.5 kbar, and the initial mineral assemblages are Grt + Melt +Ilm+ Pl + Kfs + Sill +Qz. Based on the above phase equilibrium simulation results, we define a prograde P-T path (Figure 4(b)). Phase equilibrium simulation calculations provide further information on the P-T condition of the Grenvillian felsic gneiss (T = ~870°C and P = ~9.5 kbar).

6. Zircon U-Pb geochronology, and REE and Lu-Hf isotopic characteristics

The zircon U-Pb geochronology, and the trace element and Lu-Hf isotope data of the samples can be found in Table 5–7.

It can be seen from the characteristics of the zircon cathodoluminescence (CL) images that most zircons are long columnar, with ratios of length to width of 1:1 to 3:1. The size of the zircon ranges from 30 to 150 μm, and some of the zircons have developed cracks. The CL images of most of the zircon grains show relatively

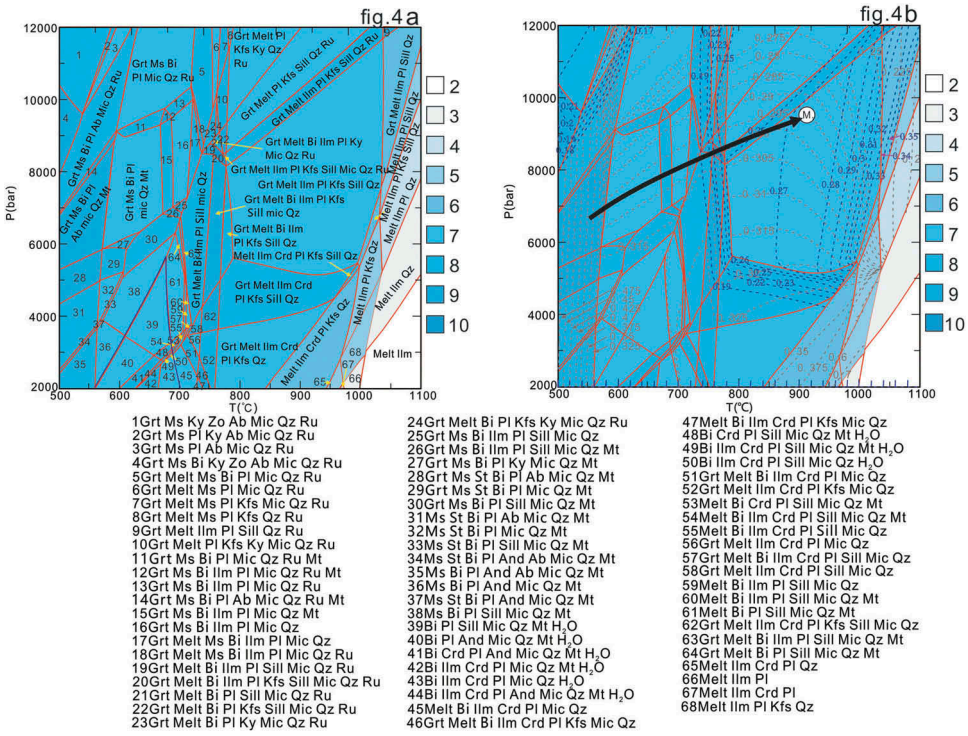

Figure 4. P-T pseudosection for the felsic orthogneiss modelled using the felsic orthogneiss composition; (b) The blue dotted line is the garnet composition isopleth (Mg# = Mg/(Fe + Mg)) ?the grey dotted line is the plagioclase composition isopleth (An = Ca/(Ca+Na +K)). The numbers next to the coloured squares represent the amount of coexisting minerals. Based on the measured mineral composition equivalent line, the maximum temperature conditions for the stability of the peak (M1) mineral combination are T = ~870°C and P = ~9.5 kbar, and on the above phase equilibrium simulation results, we define a prograde P-T path.

uniform medium intensity (grey-grey-white) overall, oscillatory zoning in the core, and a relatively broad, dark grey overgrowth (Figure 5).

In the concordia diagrams and histograms of the zircon U-Pb age from the sample, the crystallization age of the igneous precursor (protolith) to the felsic orthogneiss is ~976 Ma, and the Grenvillian metamorphic age is mainly ~899 Ma (Figure 6(a,b)). Based on the $^{207}Pb/^{235}$ U ages, Bithe 6 zircons giving ~1100 Ma ages are interpreted to be xenocrysts extracted from the country rock Some of the zircons from the sample plot in a broad discordia array that could represent a resetting of Grenvillian ages during the Pan-African event (Tong *et al*. 1995, 2019; Wang *et al*. 2008; Grew *et al*. 2012).The results of the rare earth element analysis show that the magmatic and metamorphic zircons have similar rare earth partitioning patterns, all of which show low contents of light rare earth elements, heavy rare earth element enrichment, "marked negative Eu anomalies and positive Ce anomalies (Figure 7). However, the Ce anomaly of the metamorphic zircons is not as significant as that of the magmatic zircons, and compared with the magmatic zircons, the metamorphic zircons show a less steep slope for the HREE. The magmatic zircons have a significant negative Pr anomaly, but the metamorphic zircons do not show such a feature.

The in-situ Hf isotope analysis results of the zircons are shown in Table 7. The magmatic zircons in the sample Z1220-21-1 have $^{176}Hf/^{177}$ Hf values of 0.2821～0.2822, ^{176} Lu/^{177} Hf values of 0.0007～0.0019, and εHf(t) values of −2.02 to +1.41 (mean −0.075). The t_{DM2} is 1548 ~ 1789 Ma.

7. Discussion

7.1. Geochemical characteristics of zircon trace elements and U-Pb and Lu-Hf isotope interpretations in the felsic gneiss of the Larsemann Hills

There have been a lot of studies performed on the basement complex in Prydz Bay. Isotope geochronology shows that the protolith of the basement complex intruded in 1020 ~ 1380 Ma (Sheraton *et al*. 1984; Zhao *et al*. 1995, 2003; Liu *et al*. 2007c, 2009b, 2013a, 2014; Wang *et al*. 2008; Grew *et al*. 2012). The zircon U-Pb crystallization age of the precursor to the felsic orthogneiss analysed in this study is ~ 976 Ma and it has intrusive contact relationships with the basement complex. Therefore, the formation age of the felsic gneiss is

Table 5. LA-ICP-MS zircon U-Pb data for Z1220-21-1.

Spot	Pb (ppm)	Th (ppm)	U (ppm)	Th/U	$^{207}Pb/^{235}U$	±1δ (%)	$^{206}Pb/^{238}U$	±1δ (%)	$^{207}Pb/^{235}U$ (Ma)	±1δ (%)	$^{206}Pb/^{238}U$ (Ma)	±1δ (%)
Z1220-21-1-01	130.9302	28.7422	807.7071	0.04	1.2292	0.0270	0.1307	0.0021	814	12.3155	792	11.8707
Z1220-21-1-02	193.5136	203.2081	208.9320	0.97	1.3571	0.0395	0.1419	0.0024	871	17.0023	856	13.7448
Z1220-21-1-03	86.8872	58.3525	278.2629	0.21	1.3442	0.0476	0.1315	0.0019	865	20.6287	796	10.6958
Z1220-21-1-05	193.2977	31.0255	1506.5616	0.02	0.7867	0.0450	0.0894	0.0023	589	25.5687	552	13.5317
Z1220-21-1-06	130.1413	77.6208	1097.4161	0.07	0.7132	0.0122	0.0890	0.0012	547	7.2228	549	6.9322
Z1220-21-1-07	176.4377	47.3418	874.3495	0.05	1.6102	0.0613	0.1644	0.0054	974	23.8642	981	30.1333
Z1220-21-1-08	113.2052	97.9980	271.3555	0.36	1.2156	0.0322	0.1225	0.0021	808	14.7703	745	12.2303
Z1220-21-1-09	149.1789	47.7136	797.5936	0.06	1.4623	0.0679	0.1497	0.0053	915	28.0176	900	29.8125
Z1220-21-1-10	114.0552	93.1617	216.9111	0.43	1.6614	0.0383	0.1653	0.0023	994	14.6055	986	12.6845
Z1220-21-1-11	104.1029	22.4521	1260.7985	0.02	0.6186	0.0193	0.0756	0.0019	489	12.1310	470	11.1460
Z1220-21-1-12	148.4138	140.8229	250.4559	0.56	1.4459	0.0392	0.1448	0.0033	908	16.2784	872	18.3300
Z1220-21-1-13	173.0753	56.6386	458.2472	0.12	1.8280	0.0433	0.1636	0.0041	1056	15.5483	977	22.7709
Z1220-21-1-14	111.0556	107.8346	150.6055	0.72	1.4438	0.0337	0.1507	0.0021	907	14.0125	905	11.8022
Z1220-21-1-15	167.2155	91.7852	245.7424	0.37	2.0909	0.0589	0.1781	0.0029	1146	19.3496	1056	15.7429
Z1220-21-1-16	123.9586	84.5700	246.4648	0.34	1.8251	0.0372	0.1729	0.0018	1055	13.3817	1028	9.6650
Z1220-21-1-17	104.9712	27.6709	644.1464	0.04	1.3939	0.0377	0.1432	0.0027	886	16.0112	863	15.2176
Z1220-21-1-18	119.8203	93.2488	226.0363	0.41	1.6063	0.0316	0.1547	0.0020	973	12.3128	927	11.1535
Z1220-21-1-19	134.0041	103.9079	249.2966	0.42	1.7188	0.0388	0.1674	0.0026	1016	14.4859	998	14.3252
Z1220-21-1-20	175.4564	136.7378	412.0932	0.33	1.5000	0.0314	0.1499	0.0025	930	12.7346	900	13.9428
Z1220-21-1-24	154.5005	100.9753	1085.9286	0.09	0.7920	0.0132	0.0939	0.0008	592	7.4602	579	4.9827
Z1220-21-1-25	86.9347	82.3247	300.4896	0.27	1.1530	0.0390	0.1212	0.0034	779	18.3948	738	19.3332
Z1220-21-1-26	113.6499	86.1359	297.3525	0.29	1.4245	0.0337	0.1461	0.0021	899	14.1173	879	11.6360
Z1220-21-1-27	76.1571	75.8416	224.8811	0.34	1.0635	0.0555	0.1093	0.0030	736	27.3174	669	17.5154
Z1220-21-1-28	98.3829	62.8377	307.5144	0.20	1.4506	0.0282	0.1488	0.0018	910	11.6879	894	10.3490
Z1220-21-1-29	138.6141	56.6568	1194.5052	0.05	0.9254	0.0501	0.1058	0.0046	665	26.4499	648	26.6900
Z1220-21-1-30	135.8973	98.2320	221.6388	0.44	1.9836	0.0388	0.1931	0.0023	1110	13.2075	1138	12.6724
Z1220-21-1-31	82.7281	60.7948	178.3573	0.34	1.5595	0.0312	0.1476	0.0019	954	12.3848	887	10.4098
Z1220-21-1-32	230.1534	180.4063	225.0626	0.80	1.9646	0.0482	0.1683	0.0024	1103	16.5154	1003	13.1994
Z1220-21-1-33	171.6374	104.0277	476.9187	0.22	1.5594	0.0552	0.1500	0.0040	954	21.9080	901	22.2716
Z1220-21-1-34	136.6455	103.5006	406.1711	0.25	1.3135	0.0272	0.1316	0.0015	852	11.9252	797	8.3486
Z1220-21-1-35	181.7078	88.0725	449.8798	0.20	1.9759	0.0473	0.1866	0.0026	1107	16.1391	1103	14.1706
Z1220-21-1-36	256.9907	73.6605	908.3519	0.08	1.4989	0.0335	0.1407	0.0023	930	13.6049	849	12.8961
Z1220-21-1-37	172.1957	130.2846	329.1816	0.40	1.6536	0.0297	0.1633	0.0016	991	11.3717	975	9.0799
Z1220-21-1-38	295.2227	250.3021	412.5444	0.61	1.6473	0.0312	0.1659	0.0019	989	11.9540	990	10.5539
Z1220-21-1-39	211.5964	88.7147	413.6489	0.21	2.0017	0.0317	0.1875	0.0026	1116	10.7077	1108	13.9897
Z1220-21-1-40	107.3923	84.2244	157.2936	0.54	1.7357	0.0415	0.1644	0.0017	1022	15.3985	981	9.6003
Z1220-21-1-41	139.8024	111.8419	209.5884	0.53	1.6016	0.0387	0.1680	0.0022	971	15.0978	1001	12.3551
Z1220-21-1-42	170.7990	67.7308	414.4350	0.16	1.7302	0.0480	0.1626	0.0046	1020	17.8663	971	25.4225
Z1220-21-1-44	175.0686	22.8621	943.4373	0.02	1.0028	0.0315	0.1046	0.0013	705	15.9522	641	7.3584
Z1220-21-1-45	35.2795	47.8535	216.3213	0.22	1.5118	0.0438	0.1633	0.0026	935	17.7068	975	14.4958
Z1220-21-1-46	158.9566	45.6249	1030.7487	0.04	1.1491	0.0562	0.1252	0.0047	777	26.5405	761	27.1246
Z1220-21-1-47	174.8429	157.0269	394.9871	0.40	1.1456	0.0341	0.1219	0.0024	775	16.1600	742	13.9939
Z1220-21-1-48	126.1506	20.6737	836.1207	0.02	1.1868	0.0214	0.1288	0.0015	794	9.9268	781	8.6660
Z1220-21-1-49	110.1457	98.4598	161.1776	0.61	1.5759	0.0373	0.1580	0.0024	961	14.7091	945	13.5950
Z1220-21-1-50	172.9993	60.1646	515.3282	0.12	1.8187	0.0665	0.1675	0.0051	1052	23.9625	998	28.3438
Z1220-21-1-51	179.3661	144.5091	217.3250	0.66	1.7882	0.0352	0.1729	0.0022	1041	12.8218	1028	12.1725
Z1220-21-1-52	105.6739	80.8495	127.9757	0.63	2.0011	0.0512	0.1887	0.0036	1116	17.3228	1114	19.4292
Z1220-21-1-55	115.5095	74.6856	304.8315	0.25	1.6125	0.0292	0.1603	0.0018	975	11.3679	958	9.9046

later than that of the basement felsic orthogneiss, which is consistent with the field geology. Regarding the classification of granite genesis (I-S-A), is there a systematic difference in zircon trace elements in various types of granite? Wang *et al*. (2012) made a good attempt at answering this question; they selected samples from typical I- type and S-type granites from the southern part of the Tibetan Plateau and A-type granites from the Songpan-Ganze orogenic belt on the northeastern margin of the Tibetan Plateau, and their zircon trace elements were identified in detail; their study is a good precedent for the identification of trace element characteristics of I-S-A zircons in granite, and the geochemical characteristics of granite zircons can be effectively used to discriminate rock types and tectonic environments. Plotting the Pb and Th of the magmatic zircons of the felsic orthogneiss analysed in this study shows that the sample mainly fall within the area of the S-type granitoids.

From this we conclude that the protolith of the felsic gneiss was mainly formed by the melting of pre-existing crust.

Previous studies have shown that the genesis of magmatic rocks has two modes: (1) partial melting of pre-existing crustal material, in which the εHf(t) value of the zircons in magmatic rocks will be lower than that in chondrite; (2) new crustal material or mantle material partially melted, in which the zircon εHf(t) value of magmatic rocks will be higher than that in chondrite. The εHf(t) values of the felsic gneiss sample in this paper are −2.02 to +1.41 (mean −0.075). Most of the εHf(t) of the zircons is located

Table 6. REE contents(ppm) of the zircon from the sample Z1220-21-1.

Spot	Y(ppm)	La(ppm)	Ce(ppm)	Pr(ppm)	Nd(ppm)	Sm(ppm)	Eu(ppm)	Gd(ppm)	Tb(ppm)	Dy(ppm)	Ho(ppm)	Er(ppm)	Tm(ppm)	Yb(ppm)	Lu(ppm)
Z1220-21-1-09	1195.86	0.79	4.14	0.52	2.82	2.29	0.35	16.48	7.66	105.49	37.26	161.18	35.16	321.78	52.59
Z1220-21-1-10	1463.82	0.00	0.69	0.10	2.58	7.47	0.17	41.52	13.94	150.67	49.41	192.22	37.47	327.85	50.93
Z1220-21-1-14	1660.51	0.21	3.86	0.10	1.56	4.04	0.31	27.44	11.28	139.28	55.53	250.05	55.56	523.14	86.56
Z1220-21-1-18	1926.07	0.48	4.67	0.28	1.99	2.95	0.19	22.89	10.72	154.51	64.51	310.62	70.79	687.53	117.28
Z1220-21-1-19	2427.55	0.02	2.40	0.03	0.88	3.61	0.12	31.13	13.65	192.66	81.33	383.77	86.71	841.95	140.04
Z1220-21-1-20	2867.76	0.00	1.84	0.04	0.93	3.84	0.14	33.66	15.91	229.32	93.80	458.36	102.24	979.16	164.61
Z1220-21-1-26	2194.57	0.43	3.40	0.32	2.45	4.18	0.21	29.85	13.32	186.05	74.61	337.35	75.93	709.65	118.08
Z1220-21-1-28	979.56	0.45	3.72	0.80	6.26	6.70	0.42	36.94	11.96	113.45	32.93	122.51	24.90	226.17	35.87
Z1220-21-1-31	1602.73	0.13	2.58	0.16	1.47	2.37	0.16	19.05	8.66	125.65	53.63	253.89	59.13	569.36	95.87
Z1220-21-1-33	1998.01	1.28	12.20	2.27	15.34	7.41	0.66	26.42	11.56	166.62	67.85	325.40	74.01	724.67	123.63
Z1220-21-1-37	2996.15	0.16	2.91	0.20	1.92	5.18	0.22	40.25	18.29	254.55	101.86	470.48	103.75	971.10	158.93
Z1220-21-1-38	3793.76	0.03	3.43	0.09	2.22	7.04	0.19	53.12	23.30	320.49	130.25	601.51	132.27	1231.46	202.57
Z1220-21-1-39	1456.67	6.06	37.51	7.06	41.12	14.03	1.73	32.51	11.64	140.86	46.46	193.12	40.50	348.83	57.89
Z1220-21-1-49	2284.36	0.04	3.35	0.08	1.14	4.35	0.23	31.45	13.85	189.47	77.49	363.95	80.99	796.28	131.57
Z1220-21-1-55	1663.00	0.01	0.67	0.03	0.75	3.22	0.08	25.33	11.67	151.82	54.56	242.36	50.08	468.94	73.96

Table 7. Zircon Lu-Hf isotopic compositions of the crystalline core from the sample.

Sample	$^{176}Yb/^{177}Hf$	2δ	$^{176}Lu/^{177}Hf$	2δ	$^{176}Hf/^{177}Hf$	2δ	Age(t)	$\varepsilon_{Hf}(t)$	$t_{DM(Ma)}$	$t_{DM2(Ma)}$	$f_{Lu/Hf}$
Z1220-21-1-7	0.0204	0.0008	0.0007	0.0000	0.282192	0.000015	981	0.75	1482	1630	−0.98
Z1220-21-1-10	0.0191	0.0003	0.0007	0.0000	0.282111	0.000018	1012	−1.45	1594	1765	−0.98
Z1220-21-1-13	0.0492	0.0005	0.0018	0.0000	0.282258	0.000016	976	2.27	1431	1548	−0.95
Z1220-21-1-14	0.0371	0.0012	0.0013	0.0000	0.282260	0.000017	905	1.12	1410	1549	−0.96
Z1220-21-1-16	0.0087	0.0001	0.0003	0.0000	0.282212	0.000015	1055	−9.57	1440	1738	−0.99
Z1220-21-1-35	0.0456	0.0006	0.0016	0.0000	0.282100	0.000015	1102	−0.29	1649	1789	−0.95
Z1220-21-1-38	0.0534	0.0005	0.0019	0.0000	0.282227	0.000019	989	1.39	1479	1603	−0.94
Z1220-21-1-41	0.0067	0.0007	0.0002	0.0000	0.282225	0.000015	1000	−7.34	1420	1689	−0.99

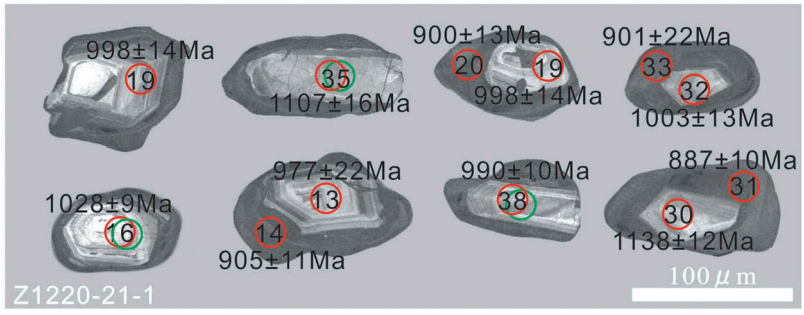

Figure 5. The CL images and the 206Pb/238 U ages of representative zircons from the sample.

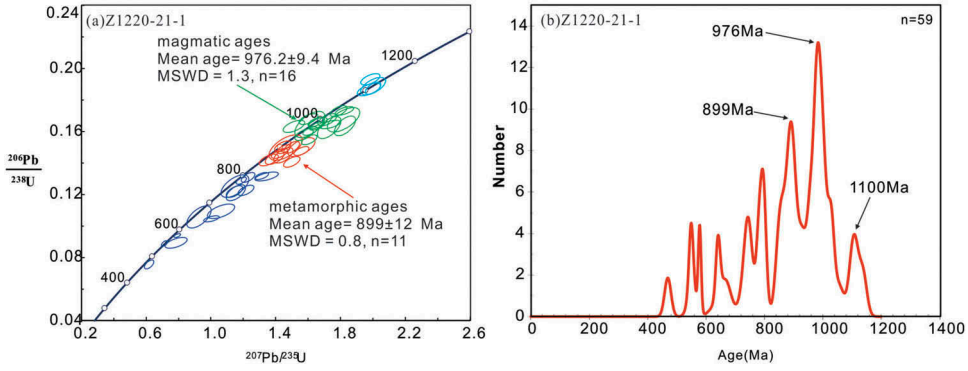

Figure 6. Concordia diagrams and histograms of zircon U-Pb age from the sample. The light blue ellipses indicate ages of the xenocrysts. The blue ellipses are related to the Pb loss.

below the chondrite line (CHUR), indicating that the source was mainly derived from partial melting of the pre-existing crust. In addition, the corresponding t_{DM2} of the felsic gneiss sample is 1548 to 1789 Ma, (Figure 8, Table 7).

Recent studies have shown that there are two episodes of high-grade metamorphism in the eastern margin of the Amery Ice Shelf, Prydz Bay. The two episodes of metamorphism occurred at 900–1000 Ma and about 530 Ma (Hensen and Zhou 1995; Wang *et al*. 2008; Liu *et al*. 2013b, 2014; Tong *et al*. 2014, 2017; Liu 2018). One of the difficulties in the study of multi-stage metamorphism superposition is the precise dating of each metamorphic event. Because the zircon U-Pb system has a high blocking temperature of > 900°C (Lee *et al*. 1997; Cherniak and Watson 2001), it is widely used in conventional isotope dating methods. However, one or more Pb loss events may result in a relatively dispersed age within the same zircon domain (Lee *et al*. 1997; Cherniak and Watson 2001; Liu 2018), and may cause the so-called 'harmonic' age to be several tens of millions of years younger than the real age (Black and Sheraton 1990; Ashwal *et al*. 1999; Yoshida 2007; Grew *et al*. 2012).

It is difficult to find a record of two-episode metamorphism in felsic gneiss because if a large number of metamorphic zircons are formed during the early granulite facies metamorphism, they are seldom formed again during later granulite phase superposition processes, especially when the temperature during the superposition is low. Even if the main mineral assemblage reaches equilibrium during the superposition process, metamorphic zircon mainly records the earlier metamorphic events because metamorphic zircon growth requires a large amount of fluid or melt, which would have already

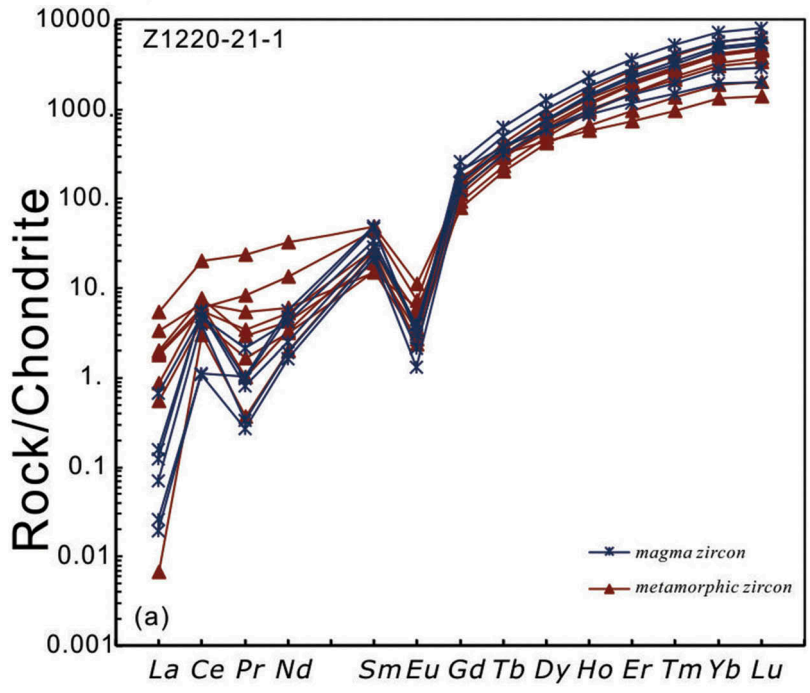

Figure 7. Chondrite-normalized REE patterns of the zircons from the sample.

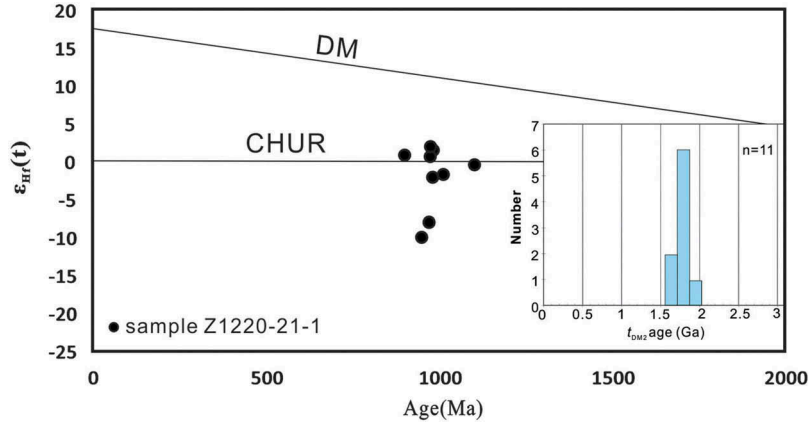

Figure 8. U-Pb age-?Hf (t) variations.

occurred during the earlier granulite facies metamorphism. In anhydrous rock, it is difficult to offer the environment suitable for zircon growth. However, if basic magmatic rocks undergo granulite facies metamorphism, a large number of metamorphic zircons will grow despite the lack of fluid. This is because in high-grade metamorphic events, metamorphism causes Zr, previously dispersed in silicate minerals to be released to form metamorphic zircons (Wei 2018). Therefore, in this study, the zircon age mainly reflects the Grenvillian tectonic thermal event, the Pan-African metamorphic age is not well recorded, but the event is reflected by those zircons in a broad discordia array (500 ~ 900 Ma) (Figure 6). This situation is common in felsic metamorphic rocks that underwent granulite facies metamorphism in the Larsemann Hills. We further precisely define the metamorphic age of the felsic gneiss in the Broknes Peninsula to be in the Grenvillian (~899 Ma).

Our experimental data and analysis supplement Wang *et al*. (2008) (Table 1), and further show that granite intrusion first occurred at ~ 976 Ma in the Larsemann Hills, followed by granulite facies metamorphism at ~ 899 Ma.

7.2. P-T path and polymetamorphism

The Prydz Belt is a typical polymetamorphic belt which underwent both Grenville and Pan-African high-grade

metamorphism (Zhang *et al*. 1996; Tong *et al*. 1998, 2002; Wang *et al*. 2008; Grew *et al*. 2012).

Since pegmatites were intruded during the Pan-African phase affecting the Larsemann Hills including the felsic orthogneiss, we conclude that the felsic orthogneiss was not immune to the thermal events of the Pan-African period. Nonetheless, our analysis of the petrology, mineral texture of metamorphic reaction characteristics, mineral chemistry, phase equilibrium simulation calculation, and zircon U-Pb dating of the felsic gneiss in the Broknes peninsula leads us to conclude that granite dehydrogenation occurred in the Grenvillian period(Grt + Ms + Bi + Pl + Ab + Mic + Qz + Mt) resulting in the formation of the currently-existing felsic gneiss (Grt + Ilm + Pl + Kfs + Sil + Qz). Because the temperature, pressure, and amount of chemically active fluids in the Pan-African period were not sufficient to change the minerals in the felsic gneiss, the mineral assemblages of the Grenvillian felsic gneiss were largely retained. In addition, due to the lack of sufficient fluid, the Pan-African thermal age is not well recorded.

7.3. Tectonic implications for the Larsemann Hills in the Grenvillian period

The Liegeois model (Liegeois 1998) clearly demarcates the period of plate convergence and describes the various stages that occurred after the end of convergence. At the same time, the plate construction settings and the periods are also clearly stated. In terms of concepts and terminology, the plate tectonics process during the convergence period is the most complete and reasonable. The subduction-accretion orogen and the continent-continent collision orogen correspond to the first and second orogenic processes of the plate convergence, respectively. The continent-continent collision orogen is the product of the convergence of the lithospheric plates.

The ocean between the two continental plates gradually closed and disappeared, and two or more land blocks were assembled and inlaid to form a unified composite continent. S-type granites are often associated with them, and the P-T trajectory of the metamorphism of the continent-continent collision orogenic belts is generally clockwise. This is manifested by the fact that the crustal thickening pressure rises to the maximum during the collision, and then, due to gravity equalization, the crust is lifted and subjected to rapid erosion, the pressure is gradually reduced, and the temperature reaches its highest point. This is followed by a period of near isothermal decompression (Li and Liu 2006). Liu *et al*. (2013b) and Tong *et al*. (2017), (2019)) discussed that the Grenvillian event in Prydz Bay and Larsemann Hills was associated with the early Neoproterozoic Rayner orogeny that was arc-continent collison.

Combined with our data, we believe that the Larsemann Hills should be categorized as the orogenic process from arc-continent collision to continent-continent collision

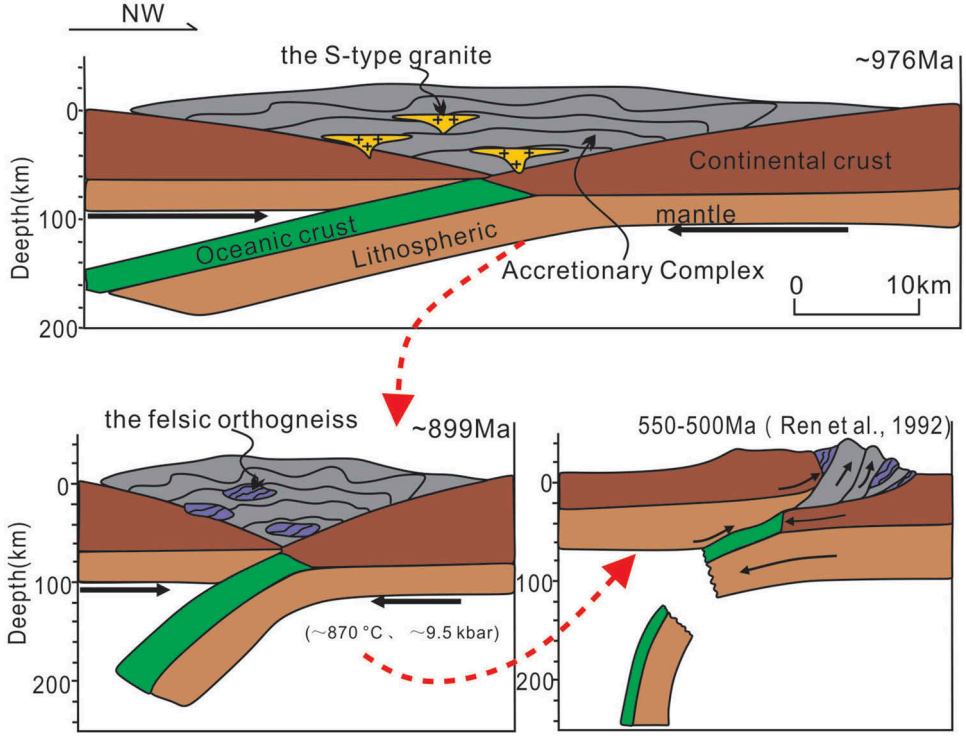

Figure 9. Simplified evolution of the Larsemann Hills, East Antarctica.

during the Grenvillian period. the arc-continent collision finished earlier than 976 Ma in the Larsemann hills, accompanied by emplacement of the S-type granite(~976 Ma), crust thickening(~899 Ma) and subsequent collapse(550–-500 Ma) (Ren *et al*. 1992) (Figure 9). The P-T condition of the feldspar orthogneiss in this study, giving rise to isothermal decompression and then isobaric cooling P-T paths, To the broader tectonic context: we infer that the East Antarctic landmass and the Indian landmass have converged and subducted at ~ 976 Ma, and the final formation time of the Rodinia supercontinent was no earlier than ~ 899 Ma.

8. Conclusions

(1) The felsic gneiss of the Broknes Peninsula intruded at ~976 Ma. The protolith was a granite (belonging to the S-type granitoid family) mainly derived from the partial melting of the lower crust.
(2) The magmatic zircons in the felsic gneiss have lower LREE and higher HREE than the metamorphic zircons.
(3) The felsic gneiss of the Broknes peninsula experienced granulite facies metamorphism in the Grenvillian period (~ 899 Ma). The metamorphic conditions were T = ~870°C and P = ~9.5 kbar.
(4) The Larsemann Hills should be categorized as the orogenic process from arc-continent collision to continent-continent collision during the Grenvillian period.
(5) The East Antarctic landmass and the Indian landmass have converged and subducted at ~ 976 Ma, and the final formation time of the Rodinia supercontinent was no earlier than ~ 899 Ma.

Acknowledgments

We thank the leaders and members of the Chinese National Antarctic Research Expedition for the logistic support during the excursions in Antarctica.

Disclosure statement

No potential conflict of interest was reported by the authors.

Funding

This research has been financially supported by the National Natural Science Foundation of China (Grant nos. 41472172, 41530209, 41941004) and a project from the Chinese Polar Environment Comprehensive Investigation and Assessment Programme (Grant no.CHINARE2015-02-05).

References

Ashwal, L.D., Tucker, R.D., and Zinner, E.K., 1999, Slow cooling of deep crustal granulites and Pb-loss in zircon - application of three microprobe techniques: Geochimica et cosmochimica acta, v. 63, p. 2839–2851. doi:10.1016/S0016-7037(99)00166-0.

Black, L.P., and Sheraton, J.W., 1990, The influence of precambrian source components on the U-Pb zircon age of a palaeozoic granite from northern Victoria Land, Antarctica: Precambrian Research, v. 46, p. 275–293. doi:10.1016/0301-9268(90)90016-J.

Boger, S.D., Wilson, C.J.L., and Fanning, C.M., 2001, Early paleozoic tectonism within the East Antarctic craton: Thefinal suture between east and west Gondwana? Geology, v. 29, p. 463–466.

Carson, C.J., Dirks, P.H.G.M., Hand, M., Sims, J.P., and Wilson, C.J.L., 1995. Compressional and extensional tectonics in low-medium pressure granulites from the Larsemann Hills, East Antarctica. Geological Magazine, v. 132, p. 151–170. doi:10.1017/S0016756800011729

Carson, C.J., Powell, R., Wilson, C.J.L., and Dirks, P.H.G.M., 1997, Partial melting during tectonic exhumation of a granulite terrane: An example from the Larsemann Hills, East Antarctica: Journal of Metamorphic Geology, v. 15, p. 105–126. doi:10.1111/j.1525-1314.1997.00059.x.

Carson, C.J., Powell, R., Wilson, C.J.L., and Dirks, P.H.G.M., 2010, Partial melting during tectonic exhumation of a granulite terrane: An example from the Larsemann Hills, East Antarctica: Journal of Metamorphic Geology, v. 15, p. 105–126. doi:10.1111/j.1525-1314.1997.00059.x.

Cherniak, D.J., and Watson, E.B., 2001, Pb diffusion in zircon: Chemical Geology, v. 172, p. 5–24. doi:10.1016/S0009-2541(00)00233-3.

Dirks, P., Carson, C., and Wilson, C., 1993, The deformational history of the Larsemann Hills, Prydz Bay: The importance of the Pan-African (500 Ma) in East Antarctica: Antarctic Science, v. 5, p. 179–192. doi:10.1017/S0954102093000240.

Dirks, P.H.G.M., and Hand, M., 1995, Clarifying temperature-pressure paths via structures in granulite from the Bolingen Islands, Antarctica: Journal of the Geological Society of Australia, v. 42, p. 16.

Fitzsimons, I., 1997. The Brattstrand Paragneiss and the Søstrene Orthogneiss: a review of Pan-African metamorphism and Grenvillian relics in southern Prydz Bay, The Antarctic Region; Geological Evolution and Processes. International Symposium on Antarctic Earth Sciences. Terra Antartica, Siena, pp. 121-130.

Fitzsimons, I.C.W., 1996, Metapelitic migmatites from brattstrand bluffs, east antarctica–metamorphism, melting and exhumation of the mid crust: Journal of Petrology, v. 37, p. 395–414. doi:10.1093/petrology/37.2.395.

Fitzsimons, I.C.W., 2000, A review of tectonic events in the East Antarctic shield and their implications for Gondwana and earlier supercontinents: Journal of African Earth Sciences, v. 31, no. 1, p. 3–23. doi:10.1016/S0899-5362(00)00069-5.

Fitzsimons, I.C.W., and Harley, S.L., 1991, Geological relationships in high-grade gneiss of the Brattstrand Bluffs coastline, Prydz Bay, East Antarctica: Australian Journal of Earth Sciences, v. 38, p. 497–519. doi:10.1080/08120099108727987.

Grew, E.S., Carson, C.J., Christy, A.G., Maas, R., Yaxley, G.M., Boger, S.D., and Fanning, C.M., 2012, New constraints from

U–Pb, Lu–Hf and Sm–Nd isotopic data on the timing of sedimentation and felsic magmatism in the Larsemann Hills, Prydz Bay, East Antarctica: Precambrian Research, v. 206–207, p. 87–108. doi:10.1016/j.precamres.2012.02.016.

Grew, E.S., Christy, A.G., and Carson, C.J., 2006, A boron-enriched province in granulite-facies rocks, Larsemann Hills, Prydz Bay, Antarctica: Geochimica et cosmochimica acta, v. 70, p. A217. doi:10.1016/j.gca.2006.06.437.

Harley, S.L., 2003, Archaean-Cambrian crustal development of East Antarctica: Metamorphic characteristics and tectonic implications, *in* Yoshida, M., B F, W., and Dasgupta, S.eds., Proterozoic East Gondwana: Supercontient assembly and breakup, London, Geol. Soc. London Special Publ, v. 206, p. 203–230.

Hensen, B.J., and Zhou, B., 1997, East Gondwana amalgamation by Pan-African collision? Evidence from Prydz Bay, East Antarctica, *in* C A, R.ed., The Antarctic region: Geological evolution and processes, Siena, Terra Antarctica Publ., p. 115–119.

Hensen, B.J., and Zhou, B., 1995. A Pan-African granulite facies metamorphic episode in Prydz Bay, Antarctica: Evidence from Sm-Nd garnet dating. 42 3.

Holland, T.J.B., and Powell, R., 2011. An improved and extended internally consistent thermodynamic dataset for phases of petrological interest, involving a new equation of state for solids Journal of Metamorphic Geology, V.29, p. 333 383.

Holland, T.J.B., and Powell, R., 1998. An internally consistent thermodynamic data set for phases of petrological interest. Journal Of Metamorphic Geology, v.16, P. 309-343.

Hou, K.J., Li, Y.H., and Tian, Y.Y., 2009, in situ U-Pb zircon dating using laser ablation-multi ion couting-ICP-MS: Mineral Deposits, v. 28, p. 481–492. in Chinese with English abstract.

Hu, J., Liu, X., Zhao, Y., Xu, G., and REN, L., 2008, Advances in the study of the orogeny and structural deformation of Prydz Tectonic Belt in East Antarctica: Acta Geoscientica Snica, v. 29, p. 343–354. in Chinese with English abstract.

Jin, X., and Zhu, H., 2000, Determination of 43 trace elements in rock samples by double focusing high resolution inductively coulpled plasma-mass spectrometry: Chinese Journal ofAnalytical Chemistry, v. 5, p. 563–567. in Chinese.

Kelsey, D., Hand, M., Clark, C., and Wilson, C., 2007, On the application of in situ monazite chemical geochronology to constraining PTt histories in high-temperature (>850 C) polymetamorphic granulites from Prydz Bay, East Antarctica: Journal of the Geological Society, v. 164, p. 667–683. doi:10.1144/0016-76492006-013.

Korhonen, F.J., Powell, R., and Stout, J.H., 2012, Stability of sapphirine + quartz in the oxidized rocks of the Wilson Lake terrane, labrador: Calculated equilibria in NCKFMASHTO: Journal of Metamorphic Geology, v. 30, p. 21–36. doi:10.1111/j.1525-1314.2011.00954.x.

Lee, J.K., Williams, I.S., and Ellis, D.J., 1997, Pb, U and Th in natural zircon: Nature, v. 390, p. 159–162. doi:10.1038/36554.

Li, M., and Liu, X., 2006, The Pan-African Prydz Belt in East Antarctica: A Col l isional orogen or an intraplate orogen: Geological Review, v. 52, p. 295–303. in Chinese with English abstract.

Li, X.W., and Wei, C.J., 2016, Phase equilibria modelling and zircon age dating of pelitic granulites in Zhaojiayao, from the Jining group of the Khondalite belt, North China Craton: Journal of Metamorphic Geology, v. 34, p. 595–615. doi:10.1111/jmg.2016.34.issue-6.

Liegeois, 1998, Somewords on the post-collisional magmatism: Lithos, p. XV XVII.

Liu, X., 2018, Deciphering multiple metamorphic events in high-grade metamorphic terranes: A case from the amery area of East Antarctica: Acta Petrologica Sinica, v. 34, p. 925–939. in Chinese.

Liu, X., Hu, J., Zhao, Y., Lou, Y., Wei, C., and Liu, X., 2009a, Late neoproterozoic/cambrian high-pressure mafic granulites from the Grove Mountains, East Antarctica: P–T–t path, collisional orogeny and implications for assembly of East Gondwana: Precambrian Research, v. 174, p. 181–199. doi:10.1016/j.precamres.2009.07.001.

Liu, X., Jahn, B.-M., Zhao, Y., Li, M., Li, H., and Liu, X., 2006, Late Pan-African granitoids from the Grove Mountains, East Antarctica: Age, origin and tectonic implications: Precambrian Research, v. 145, p. 131–154. doi:10.1016/j.precamres.2005.11.017.

Liu, X., Tong, L., Li, J., Zhao, Y., Ren, L., and Wang, Y., 1995. Tectonic evolution of East Antarctica shield during mesoproterozoic and early palaeozoic, *in* Program and Extended Abstracts, Conference on Geology across Taiwan Strait, 22-23 March, Dept. Geo l., Nat 'l Univ., Taipei, v. 2, p. 165–169. (in Chinese).

Liu, X., Xiaoxiao, L., and Bor-ming, J., 2018, U-Th-Pb monazite and Sm-Nd dating of high-grade rocks from the Grove Mountains, East Antarctica: Further evidence for a Pan-African-aged monometamorphic terrane: Advances in Polar Science, v. 29, p. 108–117.

Liu, X., Zhao, Y., and Hu, J., 2013b, The C. 1000-900 Ma and C. 550-500 Ma tectonothermal events in the Prince Charles Mountains-Prydz Bay Region, East Antarctica, and their relations to supercontinent evolution: Geological Society London Special Publications, v. 383, p. 95–112. doi:10.1144/SP383.6.

Liu, X., Zhao, Y., Hu, J., Liu, X., and Qu, W., 2013a, the grove mountains: A typical pan-african metamorphicterrane in the prydz belt, east antarctica: Chinese Journal of Polar Research, v. 25, p. 7–24. in Chinese. doi:10.3724/SP.J.1084.2013.00007.

Liu, X., Zhao, Y., Liu, X., and Hu, J., 2007b, Late neoproterozoic —early paleozoic tectonothermal events in East Antarctica: Implicationsfor amalgamation of the Gondwana supercontinent: Geological Journal of China Universities, v. 13, p. 546–560. in Chinese with English abstract.

Liu, X., Zhao, Y., Liu, X., Hu, J., and Xu, G., 2007a, Evolution of high-grade metamorphism in the Prydz Belt, East Antarctica: Earth Science Frontiers, v. 14, p. 056–063. (in Chinese with English abstract).

Liu, X., Zhao, Y., Song, B., Liu, J., and Cui, J., 2009b, SHRIMP U–Pb zircon geochronology of high-grade rocks and charnockites from the eastern amery ice shelf and southwestern Prydz Bay, East Antarctica: Constraints on late mesoproterozoic to cambrian tectonothermal events related to supercontinent assembly: Gondwana Research, v. 16, p. 342–361. doi:10.1016/j.gr.2009.02.003.

Liu, X., Zhao, Y., Zhao, G., Jian, P., and Xu, G., 2007c, Petrology and geochronology of granulites from the McKaskle Hills, Eastern amery ice shelf, Antarctica, and implications for the evolution of the Prydz belt: Journal of Petrology, v. 48, p. 1443–1470. doi:10.1093/petrology/egm024.

Liu, X.C., Wang, W., Zhao, Y., Liu, J., and Song, B., 2014, Early neoproterozoic granulite facies metamorphism of mafic

dykes from the vestfold block, East Antarctica: Journal of Metamorphic Geology, v. 32, p. 1041–1062. doi:10.1111/jmg.12106.

Liu, X.H., Zhao, Y., Liu, X., and YU, L., 2002b, Geological characteristics of the Grove Mountains in the East Antarctica——new evidence for the final suture zone of Gondwana: Science in China (Series D), v. 32, p. 457–468.

Liu, X.H., Zhao, Y., Tong, L., and Ren, L., 2002a, The East Antarctic block in the tectonic evolution of the Rodinia - Gondwana super continents: Chinese Journal of Polar Research, v. 24, p. 35–40. (in Chinese with English abstract).

Liu, Y., Gao, S., Hu, Z., Gao, C., Zong, K., and Wang, D., 2010, Continental and oceanic crust recycling-induced melt-peridotite interactions in the Trans-North China orogen: U-Pb dating, Hf isotopes and trace elements in zircons from mantle xenoliths: Journal of Petrology, v. 51, p. 537–571. doi:10.1093/petrology/egp082.

Ludwig, K.J., 2003. ISOPLOT 3.0: Berkeley Geochronology Center. Special Publication, v. 4, p. 70.

Phillips, G., Wilson, L.,.C.J., Phillips, D., and Szczepanski, K.,.S., 2007, Thermochronological ($^{40}Ar/^{39}Ar$) evidence of early palaeozoic basin inversion within the southern Prince Charles Mountains, East Antarctica: Implications for East Gondwana: Journal of the Geological Society, v. 164, p. 771–784. doi:10.1144/0016-76492006-073.

Pownall, R., Jonathan, T. E. Mark, 2015, UHT metamorphism on seram, eastern Indonesia: Reaction microstructures and P-T evolution of spinel-bearing garnet-sillimanite granulites from the kobipoto complex: Journal of Metamorphic Geology, v. 33, p. 909–935. doi:10.1111/jmg.12153.

Ren, L., Zhao, Y., Liu, X., and Chen, T., 1992, Re-examination of the metamorphic evolution of the Larsemann Hills, East Antarctica, *in* Yoshida, Y., Kaminuma, K., and Shiraishi, K. eds., Recent progress in Antarctic earth science: Tokyo, Terrapub, p.145–153.

Ren, L., Zong, S., Wang, Y., and Chong, L.I., 2018, Distribution domains of the Pan-African event in East Antarctica and adjacent areas: Advances in Polar Science, v. 29, no. 2, p. 87–107.

Sheraton, J.W., Black, L.P., and McCulloch, M.T., 1984, Regional geochemical and isotopic characteristics of high-grade metamorphics of the Prydz bay area: The extent of proterozoic reworking of Qrchaean continental crust in East Antarctica: Precambrian Research, v. 26, p. 169–198. doi:10.1016/0301-9268(84)90043-3.

Stüwe, K., and Powell, R., 1989, Low-pressure granulite facies metamorphism in the Larsemann Hills area, East Antarctica; petrology and tectonic implications for the evolution of the Prydz Bay area: Journal of Metamorphic Geology, v. 7, p. 465–483. doi:10.1111/jmg.1989.7.issue-4.

Tong, L., Jahn, B.-M., Liu, X., Liang, X., Xu, Y.-G., and Ionov, D., 2017, Ultramafic to mafic granulites from the Larsemann Hills, East Antarctica: Geochemistry and tectonic implications: Journal of Asian Earth Sciences, v. 145, p. 679–690. doi:10.1016/j.jseaes.2017.06.012.

Tong, L., Liu, X., Chen, F., Wang, Y., and Ren, L., 1995, The U-Pb zircon chronology of mafic granulite from the Larsemann Hills, East Antarctica and its possible geological implications: Antarctic Research, v. 2, p. 123–126.

Tong, L., Liu, X., Wang, Y., and Liang, X., 2014, Metamorphic P–T paths of metapelitic granulites from the Larsemann Hills, East Antarctica: Lithos, v. 192–195, p. 102–115. doi:10.1016/j.lithos.2014.01.013.

Tong, L., Liu, X., Zhang, L., Chen, H., and Chen, F., 1998, The Ar-Ar ages of hornblendes in Grt-Pl-bearing amphibolite from the Larsemann Hils,East Antarctica and their geological implication: Advances in Polar Science, v. 9, p. 1–13.

Tong, L., Liu, Z., Li, Z.-X., Liu, X., and Zhou, X., 2019, Poly-phase metamorphism of garnet-bearing mafic granulite from the Larsemann Hills, East Antarctica: P-T path, U-Pb ages and tectonic implications: Precambrian Research, v. 326, p. 385–398. doi:10.1016/j.precamres.2017.12.045.

Tong, L., Wilson, C., and Liu, X., 2002, A high-grade event of ~1100 Ma preserved within the ~500 Ma mobile belt of the Larsemann Hills, east Antarctica: Further evidence from 40Ar-39Ar dating: Terra Antarctica, v. 9, p. 73–86.

Tong, L., and Wilson, C.J.L., 2006, Tectonothermal evolution of the ultrahigh temperature metapelites in the Rauer Group, east Antarctica: Precambrian Research, v. 149, p. 1–20. doi:10.1016/j.precamres.2006.04.004.

Wang, Q., Zhu, D.C., Zhao, Z.D., Guan, Q., Zhang, X.Q., Sui, Q.L., Hu, Z. C., and Mo, X.X., 2012, Magmatic zircons from I-, S- and A-type granitoids in Tibet: Trace element characteristics and their application to detrital zircon provenance study: Journal of Asian Earth Sciences, v. 53, p. 59–66. doi:10.1016/j.jseaes.2011.07.027.

Wang, Y., Tong, L., and Liu, D., 2007. Zircon UPb ages from an ultra-high temperature metapelite, Rauer Group, East Antarctica: Implications for overprints by Grenvillian and Pan-African events, *in* Cooper, A.K., and Raymond, C.R. and The 10th ISAES Editorial Team. eds., A Keystone in a Changing World-Online Proceedings of the 10th ISAES. USGS Open-File Report 2007 — 1047, Short Research Paper 023: Reston, VA, U. S Geological Survey, v. 4.

Wang, Y., Liu, D., and Chung, S., 2008, SHRIMP zircon age constraints from the Larsmann Hills region, Prydz Bay, for a late mesoproterozoic to early neoproterozoic tectono-thermal event in East Antarctica: American Journal of Science, v. 308, p. 573–617. doi:10.2475/04.2008.07.

Wei, C., 2018, Neoarchean granulite facies metamorphism and its tectonic implications from the East Hebei terrane: Acta Petrologica Sinica, v. 34, p. 895–912(in. Chinese.

Wilson, C.J.L., Quinn, C., Tong, L., and Phillips, D., 2007, Early palaeozoic intracratonic shears and post-tectonic cooling in the rauer group, Prydz Bay, East Antarctica constrained by Ar/Ar thermochronology: Antarctic Science, v. 19, p. 339. doi:10.1017/S0954102007000478.

Yoshida, M., 2007, Geochronological data evaluation: Implications for the proterozoic tectonics of East Gondwana: Gondwana Research, v. 12, p. 228–241. doi:10.1016/j.gr.2006.10.013.

Yu, L., LIU, X., ZHAO, Y., Ju, Y., and LIU, X., 2002, Metamorphism of mafic granulites in the Grove Mountains, East Antarctica: Acta Petrologica Sinica, v. 18, p. 501–506. (in Chinese with English abstract).

Zhang, L., Tong, L., Liu, X., and Scharer, U., 1996, Conventional U-Pb ages of the high-grade metamorphic rocks in the Larsemann Hills, East Antarctica, *in* Pang, Z.ed., Advances in solid earth sciences: Beijing, Science Press, p. 27–35.

Zhao, Y., Liu, X., Song, B., Zhang, Z., Li, J., Yao, Y., and Wang, Y., 1995, Constraints on the stratigraphic age of metasedimentary rocks from the Larsemann Hills, East Antarctica: Possible implications for neoproterozoic tectonics: Precambrian Research, v. 75, p. 175–188. doi:10.1016/0301-9268(95)80005-3.

Zhao, Y., Liu, X.H., Liu, X.C., and Song, B., 2003, Pan-African events in Prydz Bay, East Antarctica, and their implications

for East Gondwana tectonics: Geological Society, London, Special Publications, v. 206, p. 231–245. doi:10.1144/GSL.SP.2003.206.01.12.

Zhao, Y., Song, B., Zhang, Z., Fu, Y., Chen, T., Wang, Y., Ren, L., Yao, Y., Li, J., and Liu, X., 1993, An early palaeozoic ('Pan-African') thermal event in the Larsemann Hills and its neighbours, Prydz Bay, East Antarctica: Science in China Press, v. 23, p. 1001–1008. (in Chinese with English abstract).

Zhou, X., Tong, L.X., Liu, X.H., Wang, Y.B., and Chen, Y.B., 2014, Metamorphism evolution of mafic granulite from the Larsemann Hills,East Antarctica: Acta Petrologica Sinica, v. 30, p. 1731–1747.